ChemComm

Accepted Manuscript

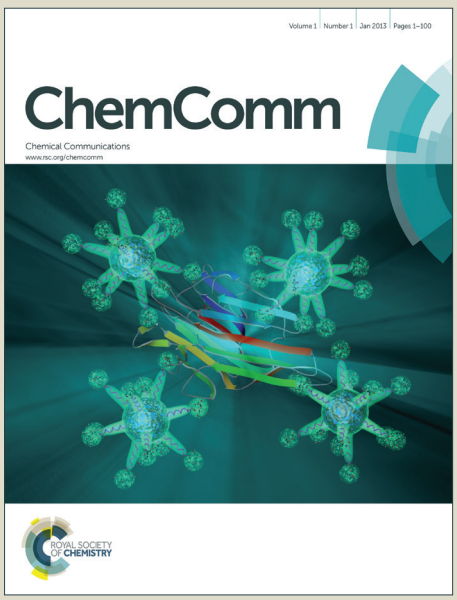

ROYAL SOCIETY OF CHEMISTRY

www.rsc.org/chemcomm

Cite this: DOI: 10.1039/c0xx00000x

www.rsc.org/chemcomm

COMMUNICATION

Defocused Differential Interference Contrast Microscopy Imaging of Single Plasmonic Anisotropic Nanoparticles†

Ji Won Ha[a,b] and Ning Fang[a,*]

Received Xth March 2014, Accepted Xth XXX 2014
DOI: 10.1039/b000000x

We present the defocused differential interference contrast (DIC) imaging of gold nanorods. We found that the scattered light and the defocus aberration play an important role in the formation of orientation-dependent DIC image patterns of a gold nanorod. Interestingly, the scattered light from a gold nanorod aligned closer to the polarization directions enables us to directly resolve its spatial orientation under a defocused DIC microscope.

Metallic nanoparticles exhibit unique size- and shape- dependent optical properties in the visible-near-infrared region of the electromagnetic spectrum resulting from surface plasmon resonance (SPR).[1-3] Among various metallic nanoparticles, gold nanorods (AuNRs) are of special interest because of their SPR spectral tunability from the visible to near-infrared by rational control of the aspect ratio.[4] This opens up many possibilities for applications such as SPR biosensing[5] and local heating for photothermal cancer therapy.[6] In particular, anisotropic AuNRs are gaining increased attention as optical orientation probes in biological imaging due to large scattering and absorption cross-sections resulting from the SPR, high photostability, and excellent biocompatibility.[7, 8]

Single particle rotational tracking using AuNR probes in biological systems is of significance to investigate certain functions and mechanisms of biomolecules that are closely related to their rotational motions.[9, 10] Several single particle orientation imaging techniques such as dark-field (DF) microscopy,[8] two-photon luminescence,[11] and photothermal heterodyne imaging[12] have been used to measure the rotational motions of single AuNRs. The most widely used technique among these methods is DF microscopy, which is based on surface plasmon scattering. However, the scattering-based DF method in biological imaging is limited by a relatively high scattering background caused by surrounding biological components, and therefore, a decrease in sensitivity. Furthermore, the scattering cross-section decreases as $1/R^6$, where R is the radius of a nanoparticle.[13] Thus, it is challenging to detect gold nanoparticles smaller than 30 nm in diameter, which sets a lower size limit even though smaller particles are desirable for biological imaging.

More recently, we reported a DIC microscopy-based single particle orientation and rotational tracking (SPORT) technique[14, 15] and a DIC polarization anisotropy method[16, 17] to resolve fast rotational dynamics of AuNRs. In DIC microscopy the incident plane-polarized beam is split by the first Nomarski prism into two orthogonally polarized mutually coherent beams (Fig. S1, ESI†). These two beams are separated by a certain distance (usually a few hundred nanometers) along the shear direction. After the two beams pass through the sample, they are recombined by the second Nomarski prism and interfere with each other. Therefore, the final DIC image of a sample results from the interference of two mutually shifted and phase-delayed beams. The two polarization directions may be defined as the bright and dark axes for imaging AuNRs (the inset of Fig. 1) according to the appearance (totally bright or dark) of DIC images when the AuNR's long axis aligns with either of the two polarization directions.

Since the interference nature of DIC microscopy makes it insensitive to the scattered light from surrounding cellular components while keeping its high-throughput capability, it is better suited to probe rotational motions of AuNRs in live cells.[18] In addition, DIC intensity (or contrast) decreases more slowly than scattering intensity as the particle size decreases.[17] Therefore, a DIC microscope provides excellent sensitivity for detecting small AuNRs in biological systems with high temporal resolution.[15-18] As an example, in the previous study we demonstrated the dynamic tracking of AuNRs (10 nm × 35 nm on average) attached to kinesin-driven microtubules,[16] which is challenging with the scattering-based methods.

Despite the recent development of DIC microscopy for tracking AuNRs, our understanding of the DIC image formation principle is still incomplete without the knowledge on the AuNR's defocused DIC image patterns. The defocused DIC orientation imaging technique, which has never been reported before, is a counterpart to the widely-used defocused DF orientation imaging technique based on the direct detection of the spatial distribution of the scattered or emitted field of single

[a] *Ames Laboratory, U.S. Department of Energy, and Department of Chemistry, Iowa State University, Ames, Iowa 50011, United States.*
[b] *Present Address: Department of Chemistry, Northwestern University, 2145 Sheridan Road, Evanston, Illinois 60208, United States.*
E-mail: nfang@iastate.edu;
Fax: +1 515 294 0105.
† Electronic Supplementary Information (ESI) available: Additioal experimental details and results. See DOI: 10.1039/b000000x/

dipoles when an aberration is deliberately applied to the imaging system.[9, 19-21] Plasmonic AuNRs much smaller than the wavelength of light have scattering cross-sections typically 4-5 orders of magnitude larger than fluorescent dye molecules.[22] The relatively strong scattered light from AuNRs can influence the DIC image patterns considerably.

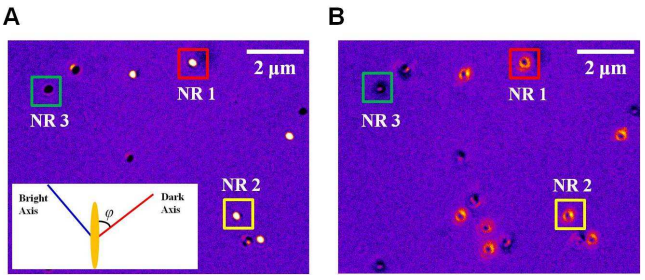

Fig. 1 Focused (A) and defocused (B) DIC images of AuNRs. Three AuNRs with different orientations were chosen and highlighted with the squares in different colors. The definition of in-plane orientation angle φ in the coordinate plane is displayed in (A).

Herein, we investigated AuNRs under a defocused DIC microscope in an attempt to better understand the effects of the scattered light and the defocus aberration on the DIC image patterns. We further tested if we could directly resolve the spatial scattering field distribution of a AuNR from a defocused DIC image.

AuNRs (25 nm × 73 nm on average) used in this study were purchased from Nanopartz (Loveland, CO, USA). A UV-Vis extinction spectrum of the AuNRs dispersed in water was collected with a Varian Cary 300 UV-Vis spectrophotometer (Fig. S2 in ESI†). The transverse SPR peak appeared at 516 nm, while the longitudinal SPR peak appeared at 700 nm. The sample was prepared by spin casting a solution containing AuNRs on a pre-cleaned glass slide to position the AuNRs relatively flat to the surface as they were fixed to the slide. The concentration of AuNRs on the glass surface was controlled to be 1 μm^{-2} in order to facilitate single AuNR characterization and to minimize inter-particle SPR coupling.

AuNRs were imaged at 700 nm, which is close to the longitudinal SPR mode. A vertical scan with a step size of ~40 nm was performed to obtain both focused (Fig. 1A) and defocused (Fig. 1B) images of randomly-orientated AuNRs immobilized on a glass slide. The orientation of a AuNR is defined as the angle φ between the AuNR's long axis and the dark polarization direction (red-line), which increases in the counterclockwise direction toward the bright polarization direction (blue-line). The DIC images taken in the focal plane (Fig. 1A) allows us to estimate the orientation of the AuNRs without further detailed intensity analysis because the bright and dark intensities are changed periodically as a function of the AuNR's orientation.[14] However, it is only possible to resolve the scattering field distribution in the defocused DIC image patterns (Fig. 1B) of the same AuNRs, which displays doughnut-shaped patterns with lobes in the peripheral area.

Fig. 2 shows the DIC images for the three AuNRs highlighted in Fig. 1 at three different defocusing distances. It is evident that the spatial field distribution of AuNR in DIC microscopy can be resolved when the sample is moved away from the focal plane. The optimum defocusing distance was determined to be ~1 μm under the DIC microscopy imaging condition to result in the clearest patterns for determining the orientation of AuNR.

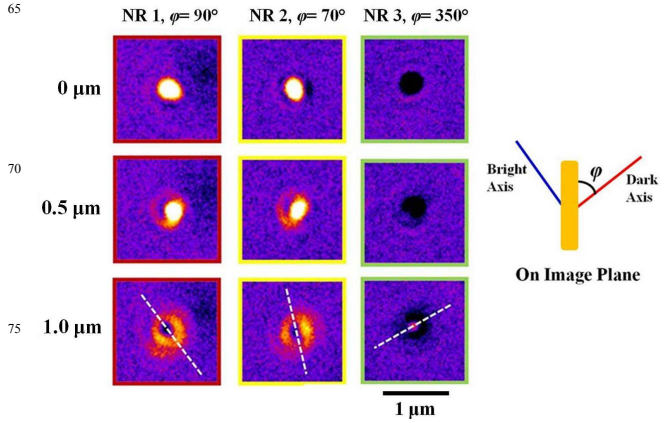

Fig. 2 DIC images for three highlighted AuNRs in Fig. 1 with defocusing distance varying from 0 μm (focal plane) to 1 μm. The white-dotted lines indicate the orientation of three AuNRs on the image plane.

At a defocusing distance of 0 μm (i.e., in-focus), the totally bright intensity observed for AuNR 1 suggests that the orientation angle φ is close to 90°, meaning the long axis of AuNR 1 is parallel to the bright polarization direction (blue-line). Details on the determination of the orientation angle of AuNRs in the focal plane are provided in ESI†. When the imaging plane was moved 1 μm away from the focal plane, a clear doughnut-shaped image pattern appeared with two lobes exhibiting the scattering field distribution and an angular anisotropy. The white-dotted line depicts the orientation of AuNR 1, yielding the orientation angle of ~90°. It should be noted that the orientation angle φ determined from the defocused DIC image shows a good agreement with the angle estimated from the focused DIC image. The orientation angle for AuNR 2 was also extracted from the defocused DIC image. The white-dotted line indicates the orientation angle of ~70° for AuNR 2, which is further supported by its focused DIC image pattern with both bright and dark portions. These results show that the scattering emanating from AuNRs contributes significantly to the DIC image patterns, which enables us to resolve their orientation angles in defocused DIC microscopy imaging. The defocusing distance is also shown to influence the DIC image patterns considerably.

Next, it is necessary to directly compare the orientation angles determined from the defocused DF and DIC microscopy imaging techniques for the same AuNRs. The comparison enables us to clearly verify the scattering field distribution shown in the defocused DIC images. Fig. 3A displays focused (top) and defocused (bottom) DF images of two AuNRs. Fig. 3B shows the correlated DIC images for the same AuNRs. In this correlation study, 1 μm microspheres allowed us to find the same particles.

The white-dotted lines show the orientation of two AuNRs in the image plane. As shown in Fig. 3, the orientation angles for the two AuNRs determined in defocused DIC microscopy imaging agreed well with those determined in defocused DF microscopy imaging. This correlation study further supports that the scattering from AuNRs is projected onto the DIC image patterns and can be directly used to resolve the orientation of AuNRs lying flat on a glass slide in the defocused DIC mode.

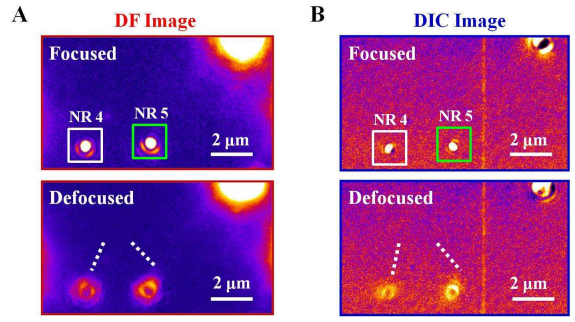

Fig. 3 Defocused DF scattering imaging *vs*. defocused DIC imaging of the same AuNRs. (A) Focused (top) and defocused (bottom) DF images of two AuNRs. (B) Focused (top) and defocused (bottom) DIC images of same AuNRs measured at the longitudinal SPR wavelength. The white-dotted lines show the orientation of two AuNRs on the image plane.

There are two important observations that need to be further discussed in the defocused DIC images of AuNRs. First, the doughnut-shaped defocused patterns show the highest contrast when a AuNR is aligned with either the bright or dark polarization direction (Fig. S3), and the contrast reduces as the AuNR rotates away from these axes. This can be explained by the polarization-dependent scattering intensity upon excitation of AuNRs with the two linearly-polarized light beams after the first Nomarski prism in a DIC microscope, which differs from the defocused DF orientation imaging method using randomly polarized light. The largely reduced intensity in the defocused DF and DIC orientation imaging methods can be a major limitation in biological experiments. Instead of using the defocused orientation imaging methods, a DIC microscopy-based in-focus orientation imaging method can be used to accurately determine the full three-dimensional (3D) orientation of in-focus AuNRs without suffering from the largely damped defocused signal intensity in biological imaging applications.[15-18]

Second, the intensity at the center of an image changes from bright to dark (or from dark to bright) as the sample moves away from the focal plane (Fig. S3). This trend was also observed for much longer Au nanowires (Fig. S4). Further theoretical studies are required to provide a more comprehensive understanding of the relationship between the defocus aberration and the DIC image patterns of plasmonic nanoparticles.

In conclusion, we demonstrated that the scattering intensity distribution of AuNRs that are oriented close to the polarization directions allows for the direct determination of the spatial orientation under a defocused DIC microscope. Our results experimentally support that the final DIC image patterns of AuNRs are considerably influenced by the scattering component, the defocus aberration, and the interference of two orthogonally polarized beams in DIC microscopy. Therefore, we provide a better understanding of the DIC image patterns of AuNRs and the factors affecting their DIC image patterns in this communication.

This work was supported by U.S. Department of Energy, Office of Basic Energy Sciences, Chemical Sciences, Geosciences, and Biosciences Division. The Ames Laboratory is operated for the U.S. Department of Energy by Iowa State University under contract no. DE-AC02-07CH11358.

Notes and references

1. S. Link and M. A. El-Sayed, *The Journal of Physical Chemistry B*, 1999, **103**, 4212-4217.
2. P. Mulvaney, *Langmuir*, 1996, **12**, 788-800.
3. J. W. Ha, K. Chen and N. Fang, *Chemical Communications*, 2013, **49**, 11038-11040.
4. C. J. Murphy, T. K. Sau, A. M. Gole, C. J. Orendorff, J. Gao, L. Gou, S. E. Hunyadi and T. Li, *The Journal of Physical Chemistry B*, 2005, **109**, 13857-13870.
5. J. Zhao, X. Zhang, C. R. Yonzon, A. J. Haes and R. P. Van Duyne, *Nanomedicine*, 2006, **1**, 219-228.
6. X. Huang, I. H. El-Sayed, W. Qian and M. A. El-Sayed, *Journal of the American Chemical Society*, 2006, **128**, 2115-2120.
7. C. J. Murphy, A. M. Gole, J. W. Stone, P. N. Sisco, A. M. Alkilany, E. C. Goldsmith and S. C. Baxter, *Accounts of Chemical Research*, 2008, **41**, 1721-1730.
8. C. Sönnichsen and A. P. Alivisatos, *Nano Letters*, 2004, **5**, 301-304.
9. E. Toprak, J. Enderlein, S. Syed, S. A. McKinney, R. G. Petschek, T. Ha, Y. E. Goldman and P. R. Selvin, *Proceedings of the National Academy of Sciences*, 2006, **103**, 6495-6499.
10. X. Zhuang, L. E. Bartley, H. P. Babcock, R. Russell, T. Ha, D. Herschlag and S. Chu, *Science*, 2000, **288**, 2048-2051.
11. T. Li, Q. Li, Y. Xu, X.-J. Chen, Q.-F. Dai, H. Liu, S. Lan, S. Tie and L.-J. Wu, *ACS Nano*, 2012, **6**, 1268-1277.
12. W.-S. Chang, J. W. Ha, L. S. Slaughter and S. Link, *Proceedings of the National Academy of Sciences*, 2010, **107** 2781-2786.
13. M. A. van Dijk, A. L. Tchebotareva, M. Orrit, M. Lippitz, S. Berciaud, D. Lasne, L. Cognet and B. Lounis, *Physical Chemistry Chemical Physics*, 2006, **8**, 3486-3495.
14. G. Wang, W. Sun, Y. Luo and N. Fang, *Journal of the American Chemical Society*, 2010, **132**, 16417-16422.
15. Y. Gu, W. Sun, G. Wang and N. Fang, *Journal of the American Chemical Society*, 2011, **133**, 5720-5723.
16. J. W. Ha, W. Sun, G. Wang and N. Fang, *Chemical Communications*, 2011, **47**, 7743-7745.
17. J. W. Ha, W. Sun, A. S. Stender and N. Fang, *The Journal of Physical Chemistry C*, 2012, **116**, 2766-2771.
18. L. Xiao, J. W. Ha, L. Wei, G. Wang and N. Fang, *Angewandte Chemie International Edition*, 2012, **51**, 7734-7738.
19. L. Xiao, Y. Qiao, Y. He and E. S. Yeung, *Analytical Chemistry*, 2010, **82**, 5268-5274.
20. M. Böhmer and J. Enderlein, *J. Opt. Soc. Am. B*, 2003, **20**, 554-559.
21. M. A. Lieb, J. M. Zavislan and L. Novotny, *J. Opt. Soc. Am. B*, 2004, **21**, 1210-1215.
22. P. K. Jain, K. S. Lee, I. H. El-Sayed and M. A. El-Sayed, *The Journal of Physical Chemistry B*, 2006, **110**, 7238-7248.